Automated System for Osteoporotic Changes Detection in Vertebral Bodies Based on CT Image Analysis

Lyakin Maksim[1[0009-0000-6022-7125]], Ilyasova Natalia[1,2[0000-0003-3027-1963]], Demin Nikita[1,2[0000-0002-8707-770X]], Alekhin Edward[3[0000-0003-3383-416X]]

[1] Samara National Research University, Moskovskoye Shosse 34, 443086 Samara, Russia
[2] Image Processing Systems Institute, NRC "Kurchatov Institute", Molodogvardeyskaya Street 151, 443001 Samara, Russia
[3] Tyumen State Medical University, Odessa Street 54, 625023 Tyumen, Russia.
lyakinm@yandex.ru

Abstract. In this work we propose an automated system for detecting osteoporotic changes in vertebral bodies from computed tomography (CT) data. The system includes spine region localisation, a deep-learning-based segmentation module (Dense U-Net) for extracting vertebral bodies, texture feature extraction (254 features including histogram, Haralick, gradient, and run-length matrix features), and machine learning classifiers for binary classification (osteoporosis vs. normal). Experimental results show that the combination of Haralick features (spatial relation 3,-3) with an SVM classifier achieves an accuracy of 0.93 on 2D spine images and 0.875 on 3D reconstructions. The software enables correction of intermediate results, supports both 2D and 3D images, and provides quantitative estimates of vertebral volume and density, assisting radiologists in early diagnosis and treatment monitoring.

Keywords: osteoporosis, CT imaging, vertebra segmentation, Dense U-Net, texture analysis, Haralick features, support vector machine.

1 Introduction

Osteoporosis is a systemic skeletal disease characterised by reduced bone mineral density (BMD) and microarchitectural deterioration, leading to an increased risk of fracture [1-3]. The disease represents a major public health problem worldwide. Vertebral compression fractures are often underdiagnosed on standard radiography - up to 47% of cases are missed [4] and only 65% are detected [5]. Figure 1 shows CT images of the lumbar spine with and without osteoporotic changes; the differences in bone texture and density are visually noticeable, yet subtle enough that even experienced radiologists may overlook early signs. With 200 million people affected worldwide and an expected 2.4-fold increase over the coming decades [6], early and accurate diagnosis is critical. Moreover, osteoporotic vertebral fractures can lead to chronic back pain, kyphosis, reduced quality of life, and increased mortality.

The WHO-recommended method, dual-energy X-ray absorptiometry (DXA), has high sensitivity but low specificity [7]. DXA also requires dedicated equipment and

trained personnel, limiting its availability in many clinics. In contrast, CT is routinely performed for other indications (e.g., chest, abdominal, or trauma scans) and offers an opportunity for opportunistic osteoporosis screening without additional radiation exposure [8-10]. Recent advances in artificial intelligence and deep learning have enabled automated analysis of medical images [11-13]. Several studies have applied convolutional neural networks to segment vertebrae and predict BMD from CT [10,14,15], while texture analysis has proven effective for characterising bone structure, which reflects trabecular microarchitecture [16-18].

Despite these advances, most existing methods focus either on segmentation or on classification, but rarely combine both in an end-to-end workflow suitable for routine clinical use. Furthermore, many approaches require high-resolution 3D data, whereas lateral CT slices are more widely available. The aim of this work is to develop and evaluate a software system that automatically segments vertebral bodies from CT images (both 2D lateral slices and full 3D volumes) and classifies them as osteoporotic or healthy using texture analysis and machine learning. The system provides a personalised approach to osteoporosis diagnosis, reduces human error, and facilitates monitoring of disease progression over time.

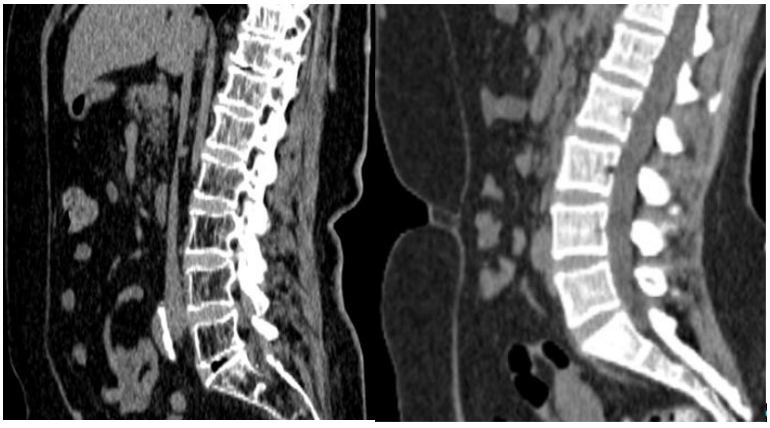

Figure 1 - CT scans of the spine with and without signs of osteoporosis

2 Technology of Vertebral Body Segmentation

Segmentation is the first and most critical step for isolating the region of interest (the spine) from surrounding tissues, such as muscles, ribs, and other organs. The workflow consists of three main stages: (1) image preprocessing to reduce noise and remove irrelevant background, (2) data augmentation to increase the effective training set, and (3) deep-learning-based segmentation using a convolutional neural network [19,20]. Each stage is described in detail below.

2.1 Dataset and Preprocessing

A total of 200 lateral CT slices from 14 patients were provided by a medical specialist (Tyumen Medical City Centre). The data were equally divided into osteoporotic and healthy groups based on subjective expert assessment using clinical criteria. Each image had a corresponding ground-truth mask created by the specialist, where white pixels denote vertebral bodies and black pixels represent all other structures. Figure 2 shows an example of an original lateral CT slice - note the presence of ribs, soft tissues, and varying contrast - and the corresponding manual mask, where the vertebral contours are precisely outlined.

All images were resized to 256×256 pixels to reduce computational load while preserving relevant anatomical details. Pixel intensities were normalised using the min-max method to the [0,1] range for stable neural network training. The dataset was split into training (80%), validation (10%), and test (10%) sets, with no patient overlap between splits. To suppress background and focus on the spinal column, each image was first cropped to remove the left and right margins, then a median filter with a 5×5 kernel was applied to reduce salt-and-pepper noise. Finally, a global binarisation step removed residual background pixels while preserving the spine region. Figure 3 displays the same image after preprocessing (cropping, filtering, and binarisation), where the spine area is clearly separated from most of the background.

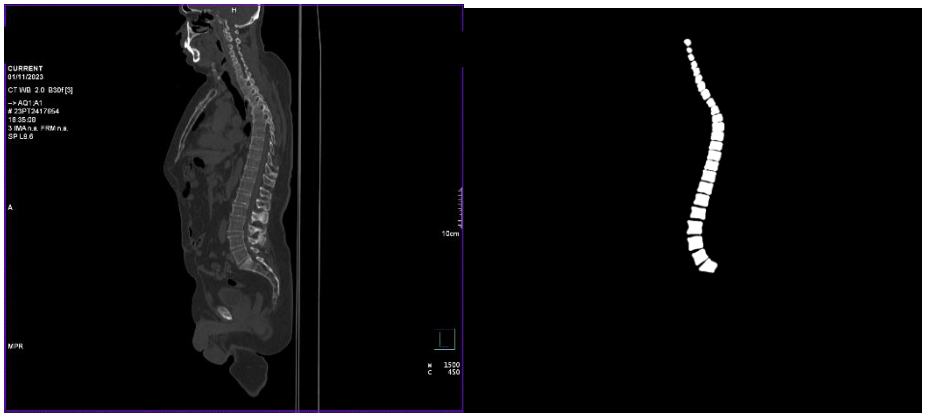

Figure 2 - Patient's lateral CT scan and its manual labeling

2.2 Neural Network Architectures

Three convolutional neural network architectures were compared, all implemented in Keras/TensorFlow [21,22]. The first is the standard U-Net [23], which consists of a contracting path (encoder) and an expansive path (decoder) with skip connections that preserve spatial information. The second is Attention U-Net [24], which adds attention gates to the decoder; these gates learn to suppress irrelevant regions and focus on salient features such as vertebral edges. The third is Dense U-Net [25], which replaces conventional convolutional blocks with dense blocks. In a dense block, each layer receives

concatenated feature maps from all preceding layers, improving gradient flow, encouraging feature reuse, and reducing the number of parameters.

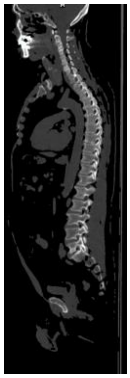

Figure 3 - Processed image

All models used the Adam optimiser with an initial learning rate of 0.001 and L2 regularisation (1e-5) to prevent overfitting. The loss function was a combination of binary cross-entropy and Dice loss (BCE Dice Loss) [26,27], which handles class imbalance well (vertebrae occupy only a small fraction of each image). Training was monitored with early stopping (patience = 20 epochs), ReduceLROnPlateau (reduces learning rate by a factor of 0.5 if the validation loss plateaus), and ModelCheckpoint (saves the best model based on the validation Dice coefficient). Figure 4 illustrates the architecture of Dense U-Net, which performed best in our experiments.

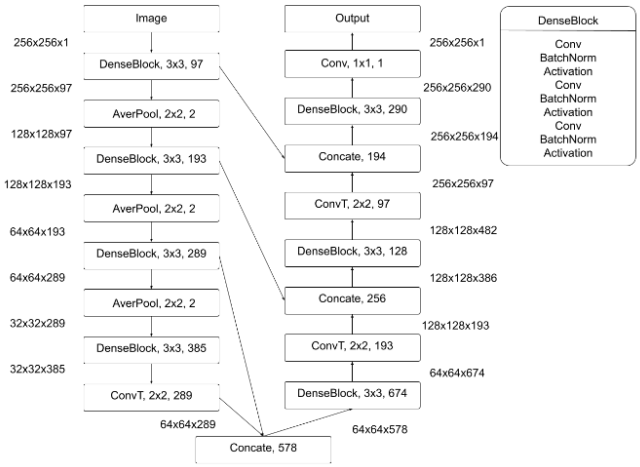

Figure 4 - Dense U-Net Network Architecture

2.3 Segmentation Results

To evaluate the quality of vertebral body segmentation we used the Dice coefficient, the standard metric for medical image segmentation. It is defined as:

$$Dice\_coef(y_{true}, y_{pred}) = \frac{2 \times \sum y_{true} \times y_{pred}}{\sum y_{true} + \sum y_{pred}},$$

where y_{pred} - predictions obtained by the model, y_{true} - the true values corresponding to these predictions.

As a loss function, we employed a combined BCE Dice Loss, which merges binary cross-entropy (BCE) and Dice loss:

$$Dice\ Loss(y_{true}, y_{pred}) = 1 - Dice\_coef(y_{true}, y_{pred}),$$

$$BCE(y_{true}, y_{pred}) = -\frac{1}{N}\sum_{i=1}^{N}\left(y_{true_i}\log(y_{pred_i}) + (1 - y_{true_i})\log(1 - y_{pred_i})\right),$$

$$BCE\ Dice\ Loss(y_{true}, y_{pred}) = Dice\ Loss(y_{true}, y_{pred}) + BCE(y_{true}, y_{pred})$$

This combination ensures stable training (BCE provides pixel-wise gradients) while focusing on the overall overlap (Dice Loss handles class imbalance well, as vertebrae occupy only a small fraction of each image).

We trained three neural network architectures (U-Net, Attention U-Net, and Dense U-Net) on the same dataset. Table 1 summarises the Dice coefficients and BCE Dice Loss values on the training, validation, and test sets.

Table 1 - Segmentation performance of the three CNN architectures

Model	Dataset	BCE Dice Loss	Dice coefficient
U-Net	Train	0.06	0.91
	Validation	0.11	0.91
	Test	0.11	0.90
Attention U-Net	Train	0.06	0.93
	Validation	0.11	0.92
	Test	0.12	0.92
Dense U-Net	Train	**0.05**	**0.96**
	Validation	**0.10**	**0.93**
	Test	**0.10**	**0.92**

The Dense U-Net achieved a Dice coefficient of 0.92 on the test set, outperforming U-Net (0.90) and matching Attention U-Net (0.92), while attaining the lowest BCE Dice Loss (0.10). Figure 5 presents the evolution of the Dice coefficient on the training set during training.

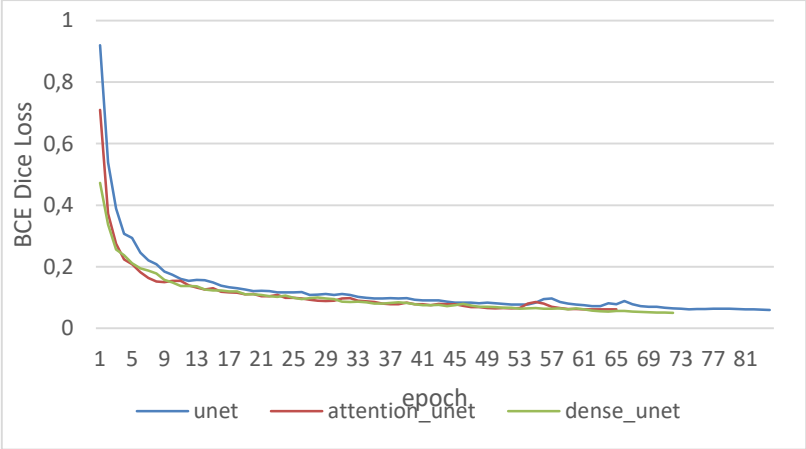

Figure 5 - BCE Dice Loss on the training data during network training

Figure 6 provides a visual comparison between a manual mask (ground truth) and the mask generated by the trained Dense U-Net. Although the automatically generated mask is not pixel-perfect - some small gaps and over-segmented areas appear - it closely follows the manual annotation, with a Dice score above 0.92. This level of accuracy is sufficient for subsequent texture analysis because the overall shape and internal structure of the vertebrae are preserved. Dense U-Net was therefore selected as the final segmentation module.

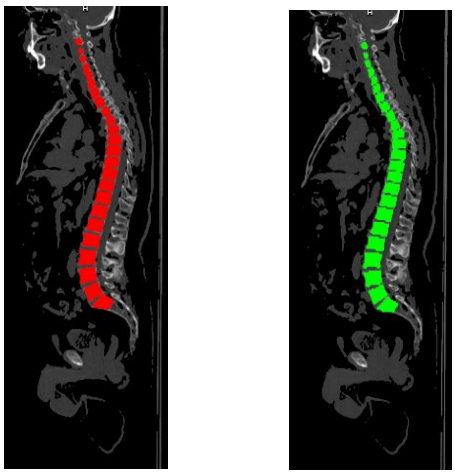

Figure 6 - Image labelled by a doctor and image labelled by the neural network

3 Technology of Texture Analysis and Classification for Osteoporosis Detection

Once the vertebral bodies are segmented, we extract a rich set of texture features that capture bone microarchitecture. Osteoporosis leads to thinning of trabeculae and increased porosity, which manifest as changes in texture patterns on CT images [16-18,28]. Unlike simple density measurements (Hounsfield units), texture features reflect the spatial arrangement of pixel intensities, making them more sensitive to early osteoporotic changes.

3.1 Feature Space Formation

For each segmented vertebra (or the whole spine region), 254 texture features were computed using custom Python code inspired by the well-known MaZda software [29]. The features are grouped into four categories [30-32]:

- Histogram features (15 features): mean, variance, skewness, kurtosis, 1st, 5th, 10th, 25th, 50th, 75th, 90th, 95th, 99th percentiles, and intensity range. These features describe the global distribution of grey levels without considering spatial relationships.
- Haralick features (220 features): based on grey-level co-occurrence matrices (GLCM) computed for 20 spatial relations (distances 1-5 pixels and angles 0°, 45°, 90°, 135°). For each GLCM, 11 Haralick parameters are calculated: angular second moment, contrast, correlation, variance, inverse difference moment, sum average, sum variance, sum entropy, entropy, difference variance, and difference entropy. These features quantify the local spatial organisation of bone texture.
- Gradient features (11 features): computed from the absolute gradient image (Sobel operator). The absolute gradient magnitude is thresholded, and statistical measures (mean, variance, skewness, kurtosis, percentiles, etc.) are extracted. These features highlight edges and sharp intensity transitions, which are altered in osteoporotic bone.
- Run length matrix features (8 features): short run emphasis, long run emphasis, grey-level non-uniformity, run-length non-uniformity, run percentage, low grey-level run emphasis, high grey-level run emphasis, and run-length variance. These features capture the coarseness or fineness of bone texture.

For 3D images, the formulas were extended to the third dimension (voxel neighbourhood in 3D), and GLCMs were computed over 3D directions.

3.2 Machine Learning Classifiers

Five supervised classifiers were trained and tuned using GridSearchCV with 3-fold cross-validation [33-37]:

- Random Forest (RF) [33]: an ensemble of decision trees that provides feature importance estimates and handles non-linear relationships well.

- Support Vector Machine (SVM) [34]: a kernel-based method that finds the optimal hyperplane separating classes; an RBF kernel was used.
- Logistic Regression (LR) [37] a linear model that estimates class probabilities; useful as a baseline.
- k Nearest Neighbours (kNN) [36]: a non-parametric method that classifies based on the majority vote of the k nearest samples.
- Gradient Boosting (GB) [35]: an ensemble that builds trees sequentially, each correcting errors of the previous one.

Hyperparameter grids were defined for each classifier, and the best combination was selected based on cross-validation accuracy. Evaluation metrics included Accuracy, Precision (positive predictive value), Recall (sensitivity), and F1-score (harmonic mean of precision and recall).

3.3 Experimental Results

First, classification was performed on individual segmented vertebrae (1759 images). Figure 7 shows an example of a single segmented vertebra after cropping to the bounding box. The best feature group for this experiment was Haralick_1_1 (distance 1, angle 0°). However, overall accuracy was low (maximum 0.82 for RF and GB). The main reasons are the small size of individual vertebrae (only about 50×150 pixels), limiting the number of pixels available for stable texture estimation, and the relatively low resolution of the original images.

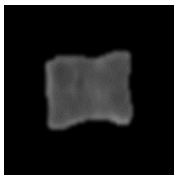

Figure 7 - Example image of a segmented vertebra

Next, classification was performed on the whole extracted spine region (200 images). Figure 8 presents an example of the whole segmented spine (posterior-anterior view) after applying the Dense U-Net mask to the original image. The spine region contains multiple vertebrae and intervertebral spaces, providing a much larger area for texture analysis. The best feature group for this task was Haralick_3_-3 (offset 3 pixels in the row direction and -3 in the column direction). Results on the test set are shown in Table 2.

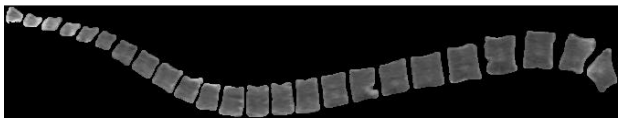

Figure 8 - Input image of segmented spine region

Table 2 - Performance of classifiers on whole-spine 2D CT images (best feature group: Haralick_3_-3).

Classifier	Accuracy	Class 0 (healthy) F1	Class 1 (osteoporotic) F1
SVM	0.93	0.94	0.92
RF	0.92	0.94	0.92
GB	0.90	0.90	0.87
LR	0.86	0.90	0.87
kNN	0.85	0.87	0.91

The SVM classifier with RBF kernel (C = 10, gamma = 'scale') achieved the highest accuracy (0.93) and balanced F1-scores. This indicates that the texture features extracted from the whole spine region are highly discriminative for osteoporosis, and the SVM model generalises well to unseen data.

3.4 3D Image Analysis

For 8 patients, full 3D CT volumes in DICOM format were available, each comprising 150-250 axial slices with a slice thickness between 1.0 and 1.5 mm. After reconstructing the 3D volume, the totalsegmentator library [38] was used to segment individual vertebrae automatically. This library is based on an nnU-Net and can label 104 anatomical structures, including all cervical, thoracic, and lumbar vertebrae. Figure 9 illustrates a full 3D reconstruction of a patient's CT scan with volume rendering and the extracted 3D spine model after segmentation, where each vertebra is colour-coded.

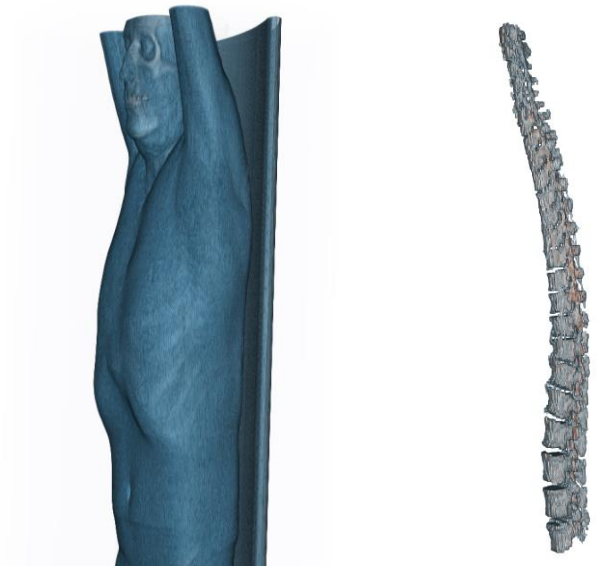

Figure 9 - Example of a 3D patient image and the 3D segmented spine

For each vertebra, 3D texture features were computed by extending the 2D formulas to three dimensions (e.g., GLCMs were computed over 13 spatial directions in 3D). The best feature group from the 2D experiments (Haralick_3_-3) was adapted to 3D (offset (3,-3,0) in the axial plane). Classification accuracy on 3D vertebrae reached 0.875 for both SVM and RF. The slightly lower accuracy compared to 2D whole-spine classification is likely due to the smaller number of 3D samples (only 8 patients, leading to fewer vertebrae). A longitudinal study of one patient who underwent CT in 2022 and 2024 showed that texture features changed inversely with volume and density: as osteoporosis progressed, volume decreased by 5-12% and density by 8-15%, while several texture features (e.g., variance, skewness) increased. This confirms that texture features capture pathological changes consistent with bone loss.

4 Computer-Aided System for Osteoporosis Diagnosis

The developed technology was implemented as a Python-based software system with a graphical user interface (GUI) using PySide6 (Qt for Python). Figure 10 presents a block diagram of the entire technology, showing the main data flow from the input CT image (2D or DICOM series) to the final classification and analysis results. The system is logically divided into four core modules:

- Segmentation module (Dense U Net) for 2D spine extraction.
- Texture feature calculation module (254 features).
- Classification module.
- 3D reconstruction and analysis module (totalsegmentator for vertebra labelling).

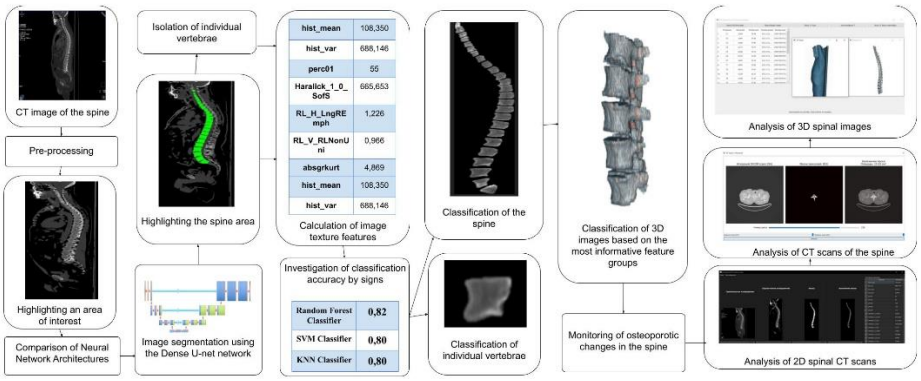

Figure 10 - Block diagram of the technology for analyzing vertebral bodies in osteoporosis

4.1 Example of Operation (2D Mode)

After launching the application, the user loads a lateral CT slice (PNG, BMP, or JPEG). The system automatically performs preprocessing (cropping, median filtering,

binarisation), then applies the trained Dense U-Net to generate a binary mask of the spine. Figure 11 illustrates the four main steps in sequence: (a) original image, (b) pre-processed image, (c) predicted mask (white = spine), and (d) final spine region extracted by overlaying the mask onto the original image. All intermediate results are shown in the interface, and the user can manually correct the mask if needed - a feature that ensures safety and flexibility in clinical use.

Once the spine region is extracted, the user clicks the “Calculate Features” button. The system computes all 254 texture features in less than two seconds (thanks to Numba acceleration). The features are presented in a scrollable table on the right side of the main window, grouped by category. The user can export the table as a CSV file for further analysis.

To classify the image, the user clicks the “Classifier” button. The system loads the pre-trained SVM model (trained on the best feature group, Haralick_3_-3) and applies it to the feature vector of the current image. A pop-up message displays the decision: “Osteoporotic changes detected” or “Normal”. The system also shows the probability of belonging to the osteoporotic class (e.g., 0.873), which can help the radiologist gauge confidence.

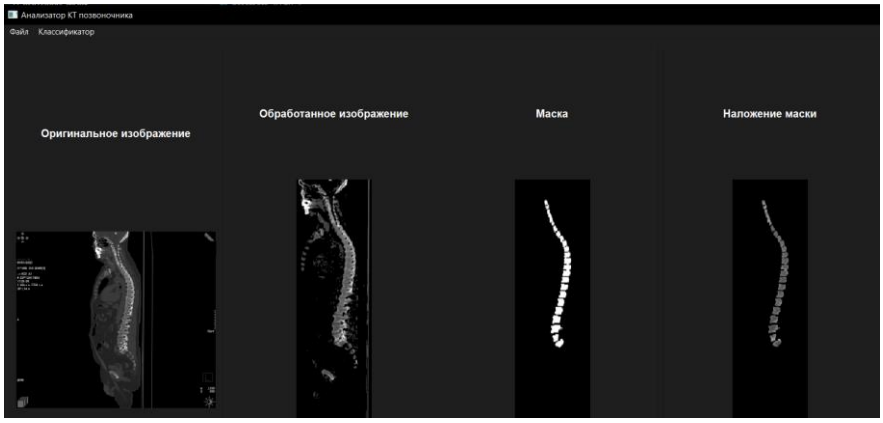

Figure 11 - Steps of spine region extraction from the original image

4.2 Example of Operation (3D Mode)

For 3D analysis, the user selects a folder containing a DICOM series of a CT scan. The system reads all DICOM files, sorts them by slice position, and reconstructs a 3D volume using the voxel dimensions from the DICOM metadata. The volume is then passed to the totalsegmentator library, which performs multi-label segmentation of the vertebrae. The segmented 3D spine model is displayed in an interactive window powered by the vedo library. Figure 12 shows this window with two panels: the full patient body (left, semi-transparent to reveal internal structures) and the isolated spine (right). Both models can be rotated, panned, and zoomed using mouse controls.

For each labelled vertebra (e.g., L1, L2, L3, L4, L5), the system computes the volume in voxels and converts it to millilitres using the voxel spacing. It also calculates the average Hounsfield unit (HU) value within the vertebra as a proxy for bone density. The system also allows inspection of individual axial slices. The user selects a slice number, and a new window opens showing three images: the original slice, the overlaid segmentation mask, and a composite view. The user can adjust the window/level (HU range) to enhance visualisation of bone structures. This feature helps radiologists verify the segmentation quality and manually correct any errors on a slice-by-slice basis if necessary.

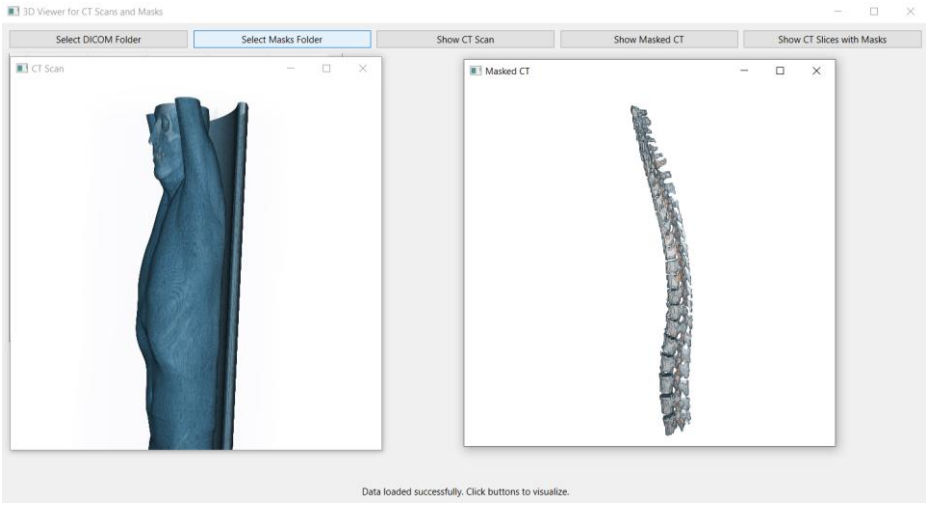

Figure 12 - Example of spine highlighting in a 3D patient image

5 Conclusions

We have developed and validated an automated technology for detecting osteoporotic changes in vertebral bodies from CT images. The key contributions of this work are as follows.

First, a segmentation method based on Dense U-Net was designed that achieves a Dice coefficient of 0.92 on lateral CT slices, outperforming standard U-Net and matching Attention U-Net while showing the lowest loss. The segmentation module runs in real time and can be manually corrected, making it suitable for clinical integration.

Second, a comprehensive texture feature set comprising 254 features from four families (histogram, Haralick, gradient, run-length) was built. By evaluating five machine learning classifiers, we found that an SVM classifier using Haralick features with spatial offset (3,-3) reaches an accuracy of 0.93 on 2D whole-spine images and 0.875 on 3D vertebrae. This demonstrates that texture analysis of whole spine regions is a viable approach for opportunistic osteoporosis screening.

Third, a software system supporting both 2D and 3D analysis modes was implemented. The system provides volume and density measurements in an intuitive graphical interface. The modular architecture allows corrections at any stage, ensuring safe and flexible operation.

The system can be used for opportunistic osteoporosis screening on routine chest or abdominal CT scans, for monitoring treatment response over time, and for reducing missed diagnoses. Future work includes expanding the dataset to hundreds of patients, integrating BMD prediction models (regression instead of classification), and validating the system in a multi-centre prospective clinical study.

Acknowledgment

The work was carried out within the state assignment of IPSI, NRC "Kurchatov institute".

References

1. Lesnyak, O.M., Benevolenskaya, L.I.: Osteoporosis: diagnosis, prevention, treatment. GEOTAR-Media, Moscow (2010) (in Russian)
2. Chadha, M., et al.: Osteoporosis: Epidemiology, Pathogenesis, Evaluation and Treatment. Open J. Orthop. 12(4), 153-182 (2022)
3. Kostyuchek, D.F., et al.: Early diagnosis of osteoporosis in women. J. Obstet. Womens Dis. 55(1), 3-7 (2006) (in Russian)
4. Cook, G.J., et al.: The value of bone scintigraphy in the evaluation of osteoporotic patients with back pain. Scand. J. Rheumatol. 31(4), 245-248 (2002)
5. Takahara, K., et al.: Radiographic evaluation of vertebral fractures in osteoporotic patients. J. Clin. Neurosci. 14(2), 122-126 (2007)
6. Verbovoy, A.F., et al.: Osteoporosis: current state of the problem. Ther. Arch. 89(5), 90-97 (2017) (in Russian)
7. Sivkov, A.V., et al.: Osteoporosis in hormonal therapy of prostate cancer and bone remodeling markers. Exp. Clin. Urol. (4), 46-53 (2015) (in Russian)
8. Buckens, C.F., et al.: Osteoporosis markers on low dose lung cancer screening chest computed tomography scans predict all cause mortality. Eur. Radiol. 25(1), 132-139 (2015)
9. Yasaka, K., et al.: Prediction of bone mineral density from computed tomography: application of deep learning with a convolutional neural network. Eur. Radiol. 30, 3549-3557 (2020)
10. Petryaykin, A.V., et al.: Artificial intelligence technology for vertebral compression fracture recognition using a morphometric analysis model based on convolutional neural networks. Probl. Endocrinol. 66(5), 48-60 (2020) (in Russian)
11. Li, X., et al.: Role of Artificial Intelligence in Medical Image Analysis: A Review of Current Trends and Future Directions. J. Med. Biol. Eng. 44, 231-243 (2024)
12. Halavataya, K.A., Kozadaev, K.V., Sadau, V.S.: Adjusting videoendoscopic 3D reconstruction results using tomographic data. Comput. Opt. 46(2), 246-254 (2022)
13. Gusev, A.V.: Perspectives of neural networks and deep machine learning in creating healthcare solutions. Doctor IT (3), 92-105 (2017) (in Russian)

14. Beskrovny, A.S., et al.: Using a convolutional neural network to automate the construction of two dimensional solid state vertebra models. Izv. Saratov Univ. Math. Mech. Inform. 20(4), 502-516 (2020) (in Russian)
15. Seo, J.W., et al.: A deep learning algorithm for automated measurement of vertebral body compression from X ray images. Sci. Rep. 11, 13732 (2021)
16. Velma, K.M., Dovgyallo, Y.V., Kalashnikova, E.A., Gorbacheva, E.A.: Prospects of texture analysis for assessing bone structure. Far East Med. J. (3), 141-145 (2024) (in Russian)
17. Kapishnikov, A.V., Pervushkin, S.S.: Texture analysis in assessing bone structure and predicting osteoporotic femoral neck fractures. Bull. Russ. Sci. Cent. Radiol. 15(1), 1-16 (2015) (in Russian)
18. Sollmann, N., et al.: Texture Analysis Using CT and Chemical Shift Encoding Based Water Fat MRI Can Improve Differentiation Between Patients With and Without Osteoporotic Vertebral Fractures. Front. Endocrinol. 12, 778537 (2022)
19. Yurova, A.S.: Methods for automated segmentation of CT images of the abdominal cavity. PhD thesis, Lomonosov Moscow State University, Moscow (2018) (in Russian)
20. Al Temimi, A.M.S., Pilidi, V.S., Ibraheem, M.K.I.: Novel approach of simplification detected contours on X ray medical images. Comput. Opt. 46(3), 479-482 (2022)
21. Berbasov, V.D.: Comparative review of Keras and PyTorch neural network libraries. Ekon. Sotsium (8(111)), 423-426 (2023) (in Russian)
22. Chicho, B.T., Sallow, A.B.: A Comprehensive Survey of Deep Learning Models Based on Keras Framework. J. Soft Comput. Data Min. 2(2), 49-61 (2021)
23. Ronneberger, O., Fischer, P., Brox, T.: U Net: Convolutional Networks for Biomedical Image Segmentation. arXiv 1505.04597 (2015)
24. Oktay, O., et al.: Attention U Net: Learning Where to Look for the Pancreas. arXiv 1804.03999 (2018)
25. Cai, S., et al.: Dense UNet: a novel multiphoton in vivo cellular image segmentation model based on a convolutional neural network. Quant. Imaging Med. Surg. 10(6), 1275-1285 (2020)
26. Getmanskaya, A.A., Sokolov, N.A., Turlapov, V.E.: Multiclass U Net segmentation of brain electron microscopy using original and semi synthetic training datasets. Programmirovanie (3), 22-29 (2022) (in Russian)
27. Shishkova, V.A., Gromov, N.V., Mironycheva, A.M., Kirillin, M.Y.: Segmentation of three dimensional human skin OCT images using U Net neural networks. Mod. Technol. Med. 17(1), 6-17 (2025) (in Russian)
28. Ilyasova, N.Yu., Shirokanev, A.S., Kupriyanov, A.V., Paringer, R.A.: Technology of intellectual feature selection for a system of automatic formation of a coagulate plan on retina. Comput. Opt. 43(2), 304-315 (2019)
29. Strzelecki, M., Szczypinski, P., Materka, A., Klepaczko, A.: A software tool for automatic classification and segmentation of 2D/3D medical images. Nucl. Instrum. Methods Phys. Res. A 702, 137-140 (2013)
30. Kovalev, I.L.: Texture features of images. BNTU, Minsk (2010) (in Russian)
31. Yakovleva, E.V., Nesterova, E.P.: Comparative analysis of Laws and co occurrence matrix methods in texture image segmentation. Prikl. Radioelektron. 8(2), 181-187 (2009) (in Russian)
32. Ilyasova, N.Yu., Paringer, R.A., Ushakova, N.S., Kupriyanov, A.V.: Intelligent feature selection for localisation of objects in fundus images based on colour subspace analysis. In: Proc. ITNT 2017, pp. 1740-1746. Samara (2017) (in Russian)
33. Chistyakov, S.P.: Random forests: a review. Tr. Karel. Nauch. Tsentra RAN (2), 117-136 (2013) (in Russian)

34. Abdullah, D.M., Abdulazeez, A.M.: Machine Learning Applications based on SVM Classification: A Review. Qubahan Acad. J. 1(2), 81-90 (2021)
35. Karkare, P.: The Artistry of Stochastic Gradient Boosting and Gradient Boosting Classifiers in Chronic Renal Disease Classification. J. Electr. Syst. 20(3), 2405-2415 (2024)
36. Abu Aisheh, Z., Raveaux, R., Ramel, J.Y.: Efficient k nearest neighbors search in graph space. Pattern Recognit. Lett. 134, 77-86 (2020)
37. Ranganathan, P., Pramesh, C.S., Aggarwal, R.: Common pitfalls in statistical analysis: Logistic regression. Perspect. Clin. Res. 8(3), 77-86 (2017)
38. Wei, L., et al.: Development and Validation of Multi Omics Thymoma Risk Classification Model Based on Transfer Learning. J. Digit. Imaging 36, 2015-2024 (2023)